NANO LETTERS

pubs.acs.org/NanoLett

Properties of Fluorinated Graphene Films

Jeremy T. Robinson,* James S. Burgess, Chad E. Junkermeier, Stefan C. Badescu, Thomas L. Reinecke, F. Keith Perkins, Maxim K. Zalalutdniov, Jeffrey W. Baldwin, James C. Culbertson, Paul E. Sheehan, and Eric S. Snow

†Naval Research Laboratory, Washington, D.C. 20375

ABSTRACT Graphene films grown on Cu foils have been fluorinated with xenon difluoride (XeF_2) gas on one or both sides. When exposed on one side the F coverage saturates at 25% (C_4F), which is optically transparent, over 6 orders of magnitude more resistive than graphene, and readily patterned. Density functional calculations for varying coverages indicate that a C_4F configuration is lowest in energy and that the calculated band gap increases with increasing coverage, becoming 2.93 eV for one C_4F configuration. During defluorination, we find hydrazine treatment effectively removes fluorine while retaining graphene's carbon skeleton. The same films may be fluorinated on both sides by transferring graphene to a silicon-on-insulator substrate enabling XeF_2 gas to etch the Si underlayer and fluorinate the backside of the graphene film to form perfluorographane (CF) for which calculated the band gap is 3.07 eV. Our results indicate single-side fluorination provides the necessary electronic and optical changes to be practical for graphene device applications.

KEYWORDS Graphene, fluorine, perfluorographane, graphene fluoride, functionalization

The fluorination of sp^2 carbon dates back decades, first with bulk graphite[1−3] and later with buckeyballs[4] and carbon nanotubes.[5−7] Graphite fluoride attracted interest for technological applications such as lubricants,[8] and as a result, numerous experimental[3,9,10] and theoretical[11,12] studies exist describing its synthesis and properties. The basic building block of graphite fluoride—referred to as graphite monofluoride $(CF)_n$ or carbon monofluoride—is in vogue again, due to the recent scientific and technological interest in graphene.[13,14] Beyond its potential for lubrication, fluorination of graphene enables its electronic properties to be tuned for modern electronics. In particular, band gap engineering through chemical modification is attractive since it is both scalable and inexpensive.[15] Moreover, by analogy with fluorinated carbon nanotubes, fluorination should also enable multiple robust reaction pathways for subsequent chemical modification. In this work we describe a facile route to fluorinate graphene, form large cm^2 sheets of graphite monofluoride $(CF)_n$ (referred to here as perfluorographane) and discuss their resulting properties.

A number of techniques have been used to fluorinate sp^2 carbon, including exposure to F_2 gas at moderate temperatures (400−600 °C)[1,2] and treatment with F-based plasmas.[16,17] In the present work we combine advances in large-area graphene growth and fluorine-based etching of silicon to fluorinate graphene at room temperature. Xenon difluoride (XeF_2) isotropically etches silicon and can fluorinate carbon nanotubes.[18] We show that XeF_2 is a strong fluorinating agent for graphene without etching, thereby providing a facile route for graphene functionalization. Characterization of this process via X-ray photoelectron spectroscopy (XPS) and Raman spectroscopy reveals room-temperature fluorination saturates 25% coverage (C_4F) for single-sided exposure and CF for double-sided exposure. Transport measurements show C_4F is significantly more resistive (by a factor of 10^6) than graphene, which suggests the feasibility of patterning electronic pathways by removing conductivity as opposed to removing conductor. Finally, we also use density functional theory (DFT) calculations to show the C_4F structure is the lowest energy configuration for single-sided fluorination and that an appreciable band gap opens even at low fluorine coverages.

Graphene films were grown on Cu foils then transferred to either silicon-on-insulator (SOI) or SiO_2/Si substrates using techniques described by Li et al.[19] Transferred graphene samples were subsequently annealed up to 400 °C in forming gas to further remove residues.[20] The graphene films contain wrinkles as well as isolated multilayers covering no more than 5% of the film.[19] Graphene fluorination occurred in a Xactix® XeF_2 etching system, where XeF_2 gas exposure times ranged from 30 to 1200 s at approximately 30°C. Defluorination was carried out using hydrazine vapor and mild thermal annealing between 100 and 200 °C using a system described elsewhere.[21] DFT calculations of the electronic and structural properties of these systems were made using a plane wave code[22] with GGA with the PBE exchange-correlation, Vanderbilt ultrasoft pseudopotentials,[23] a kinetic energy cutoff energy of 300 eV, and Brillouin zone sampling with a Monkhorst−Pack mesh. For unfluorinated graphene, this approach gave the usual zero gap semimetal with a band crossing at the K point of the Brillouin zone.[24] It also gives a lattice constant $a = 4.65$ atomic units in agreement with experiment[25] and with other calculations.[24]

* To whom correspondence should be addressed, Jeremy.robinson@nrl.navy.mil.
Received for review: 04/23/2010
Published on Web: 07/16/2010

DOI: 10.1021/nl101437p | *Nano Lett.* **2010,** *10,* 3001–3005

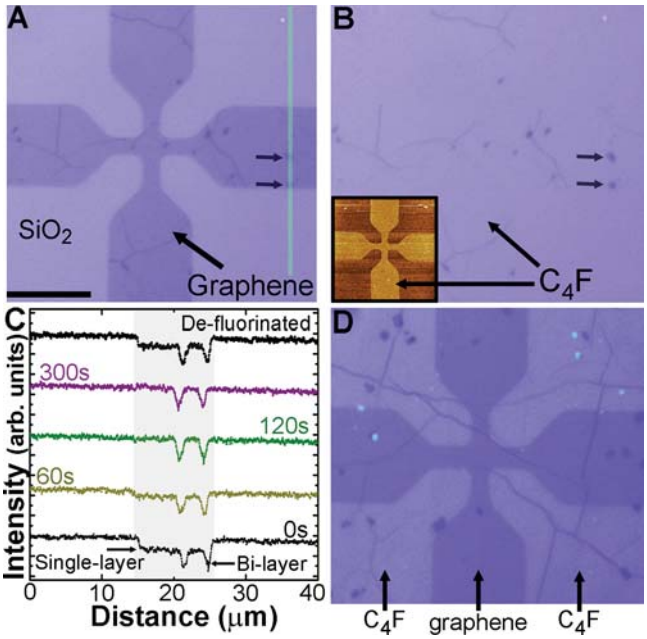

FIGURE 1. Optical changes of graphene upon fluorination. Optical micrograph (A) before and (B) after single-side fluorination on SiO_2 (SiO_2 thickness = 100 nm, scale bar = 10 μm). The expected etch rate of thermal SiO_2 with XeF_2 gas under these conditions is negligible (<0.1 nm).[29,30] (B inset) AFM height image after single-side fluorination. The height of the film after patterning and fluorination is ~1.0−1.5 nm. (C) The green component of the RGB signal taken along the green line in (A) from top to bottom, recorded with a CCD camera. The small arrows in (A) and (B) mark the location of the bilayer regions shown in (C). Profiles were taken at varying exposure times to XeF_2 and after defluorination (labeled above each profile). (D) A different graphene film selectively patterned with fluorine (note: image is contrast enhanced; dark central cross is graphene; light regions are partially fluorinated graphene).

Exposing graphene to XeF_2 gas results in fluorine chemisorption, which dramatically changes the film's optical and electronic properties. Most immediately evident is a disappearance of optical contrast upon fluorination, suggesting an insulating nature for fluorinated graphene (Figure 1). Optical transparency and low conductivity also occur when bulk graphite fluoride is formed from graphite, which appears white[26] due to scattering from interfaces within the bulk. In Figure 1A an as-fabricated graphene Hall cross structure shows three regions of optical contrast: single-layer graphene, bilayer graphene, and wrinkles in the film. Upon fluorination of the top surface to C_4F, contrast from the single-layer regions disappears and only that from the bilayer regions and the wrinkles remain (Figure 1B). Atomic force microscopy (AFM) confirms the film is not etched after XeF_2 treatment (Figure 1B). The optical absorption of graphene is quantized with each layer[27,28] and as the surface is fluorinated here, absorption equivalent to single-layer graphene remains at the bilayer regions (Figure 1C). The complete loss of contrast for single-layer but not bilayer graphene indicates that fluorine chemisorption occurs only at the surface and does not intercalate between layers under these conditions. We exploit this to pattern graphene films with fluorine as shown in Figure 1D. Here, part of the film was protected with photoresist during XeF_2 exposure.

Due to its high electronegativity, fluorine induces strong chemical shifts in the carbon 1 s binding energy allowing the use of X-ray photoelectron spectroscopy (XPS) to quantify composition and bonding type. Two types of samples were fabricated to characterize the fluorination process: (i) graphene on Cu for single-side fluorination and (ii) graphene on silicon-on-insulator (SOI) for double-side fluorination. As mentioned earlier, XeF_2 gas preferentially etches silicon. Pinholes in graphene that are naturally occurring allow the passage of XeF_2 to etch the Si and fluorinate the backside of the graphene film (inset Figure 2A). Figure 2A shows the percent fluorination for the single-side and double-side fluorinated samples, as well as the percent silicon left in the top silicon layer of the SOI substrate during XeF_2 exposure. Graphene on Cu is the "cleanest" system having no adventitious carbon contamination from adhesive tapes or PMMA. Under these fluorination conditions the fluorine content linearly increases (triangles in Figure 2A) with exposure time until 90 s, after which the concentration saturates at 20 atom % F (25% coverage or C_4F). This corresponds to one fluorine atom per every two primitive graphene unit cells in graphene.

We have made calculations for several single-sided periodic arrangements of fluorine atoms on graphene for a number of different coverages.[32] Results for the binding energy per F atom[33] for the configuration with the lowest total energy for each coverage is shown in Figure 3A. The binding energy is largest for the 25% coverage (C_4F), which is consistent with the 25% coverage observed in experiment (Figure 2A). This configuration is shown in Figure 3B and has F atoms at third nearest neighbor sites (resulting in isolated pi resonances), a configuration shown to be favored for carbon nanotubes (CNTs).[33] However, unlike graphene, the minimum energy coverage for CNTs is C_2F, where the curvature of the CNT surface favors a close packing of fluorine atoms that form "bands" along the tube axis.[33,34]

The fluorination of graphene on SOI (preannealed at 400 °C) proceeds to the same concentration as that on copper for the first 90 s of exposure, after which the fluorine content increases and saturates at 50 atom % (black circles in Figure 2A). This concentration corresponds to two fluorine atoms in each unit cell and an empirical structure of CF. Simultaneous to the sharp rise in fluorine levels, XeF_2 begins to etch the silicon underlayer (red circles in Figure 2A) as shown in the inset of Figure 2A. At this point, the backside of the graphene film has access to XeF_2 for fluorination. XPS analysis of the carbon spectrum after fluorine saturation at 50 atom % shows the majority of bonding is C−F (~86%), with a smaller fraction of $C-F_2$ (~12%) and $C-F_3$ (~2%) (Figure 2C). The formation of $C-F_2$ and $C-F_3$ on graphene would occur at defects such as vacancies, free edges, or domain boundaries. We note the graphene transfer process can also introduce defects, and we observe larger quantities of $C-F_x$ ($x > 1$) species for these samples compared to the

DOI: 10.1021/nl101437p | *Nano Lett.* **2010,** *10,* 3001–3005

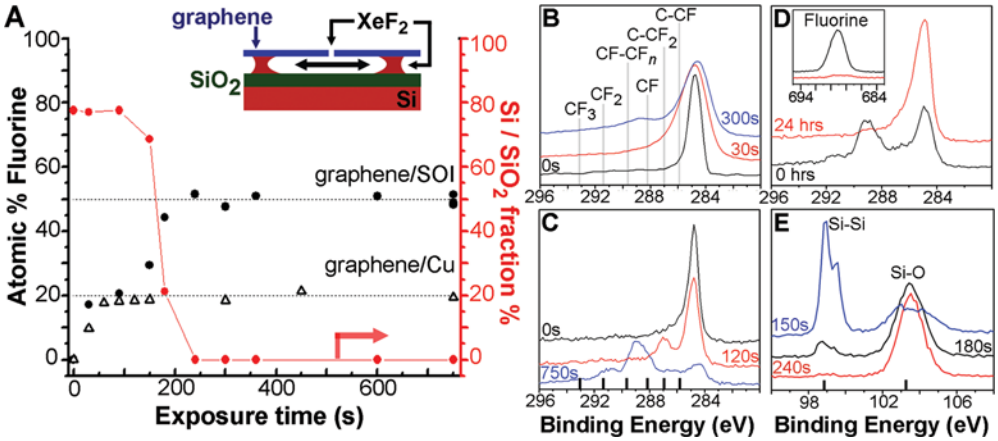

FIGURE 2. X-ray photoelectron spectroscopy (XPS) analysis of fluorine functionalization during XeF_2 exposure. (A) Fluorine fraction for single (graphene/Cu) and double (graphene/SOI) side exposure to XeF_2 for different samples. The silicon fraction refers to the percent silicon left in the top silicon layer of the SOI stack and was estimated by taking the ratio of the Si−Si peak area (99 eV) to the Si−Si plus Si−O peak area (103.5 eV) (panel E). (inset) Cartoon showing Si underlayer etching through a pinhole and edges in the graphene film on SOI. Individual XPS carbon spectra from (A) are shown in (B) and (C). (B) XPS carbon spectra after XeF_2 exposure of graphene on Cu. Several carbon−fluorine components are labeled.[31] (C) XPS carbon spectra after XeF_2 exposure of graphene on SOI. (D) XPS carbon spectra illustrating defluorination after hydrazine vapor exposure. (inset) Fluorine peak before and after 24 h hydrazine treatment. (E) XPS silicon spectrum from (A) showing evolution of Si−Si peak during XeF_2 etching.

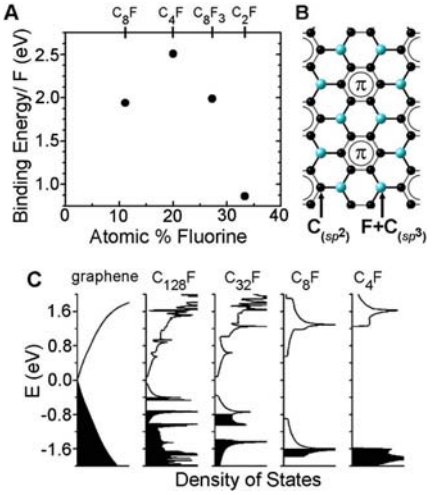

FIGURE 3. (A) Calculated binding energy per F atom compared to the F_2 gas state. (B) Sketch of the calculated C_4F configuration for the 25% coverage from (A). (C) Calculated total density of states of single-side fluorinated graphene for several fluorine coverages.

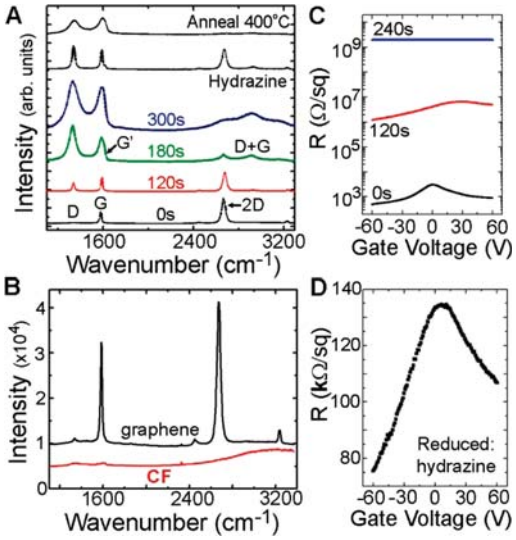

FIGURE 4. (A) Raman spectrum of graphene during single-side fluorination and defluorination on SiO_2 ($\lambda = 532$ nm). Defluorination via hydrazine vapor (24 h at ~100 °C) and thermal annealing (400 °C for 1 h in H_2/Ar gas) is shown for comparison. (B) Raman spectrum comparing graphene on SiO_2 and perfluorographane formed on SOI. The spectra are offset for clarity. (C) Example of the resistance per square vs gate voltage curve for a typical graphene device exposed to XeF_2 at different times. The 240 s exposure nominally represents C_4F. (D) Resistance per square vs gate voltage of the device in (C) after exposure to hydrazine vapor for 18 h. The hole field-effect mobility (μ_{FE}) changed from $\mu_{FE} = 1060$ cm^2/(V s)[38] to ~5 cm^2/(V s) before fluorination and after defluorination, respectively.

fluorination of graphene on copper. Importantly, these multiply fluorinated carbons will contribute more to nonreversibilities toward a pristine graphene structure. During thermal defluorination of doubly fluorinated carbons, the products can evolve as C_2F_4 instead of fluorine alone.[9]

Changes in the Raman spectra also are dramatic during fluorination. During single-side fluorination, the characteristic disorder-induced peak (D peak) at 1350 cm^{-1} appears as fluorine chemisorbs on the surface (Figure 4A). The ratio of the 2D peak (2680 cm^{-1}) to G peak (1580 cm^{-1}) drops significantly, while both the D′ (1620 cm^{-1}) and the D + D′ (2950 cm^{-1}) peaks broaden, to the point where they overlap with the G and 2D peak, respectively. This transition—increasing D and D′ peaks, broadening G peak, and decreasing 2D peak—corresponds to a high degree of structural disorder. Indeed, after a 5 min XeF_2 exposure the Raman spectra look more like that from highly disordered or nanostructured carbon-based materials.[35,36] When fluorinated to a concentration of 50 atom % F, the Raman signature is almost completely quenched (Figure 4B). This indicates

DOI: 10.1021/nl101437p | Nano Lett. 2010, 10, 3001–3005

virtually no sp^2 coordinated carbon remains after double-side fluorination. For these experiments the small fraction of sp^2 domains that remain will mostly be constrained to multilayer regions, such as that observed in Figure 1.

Calculations were made for the system with full fluorination on both sides (CF), which has two F atoms per graphene unit cell, one on each side. The fully fluorinated system is an insulator with a band gap of 3.07 eV, in agreement with previous calculations.[37] It is a regular periodic structure, with different electronic properties than graphene and no defects. These properties are consistent with the absence of G and D features in the Raman spectra in Figure 4B.

The Raman data of the defluorinated material (Figure 4A) show that graphene recovery is not complete, potentially due to carbon loss from the skeleton during defluorination. Thermal reduction between 300−400 °C removes fluorine but also apparently loses significant carbon as indicated by the relatively unchanged Raman spectra before and after defluorination (Figure 4A and Supporting Information). Carbon loss is observed in bulk thermal defluorination of graphite fluoride at 400−600 °C where carbon−fluorine products such as CF_4, C_2F_4, and C_2F_6 evolve from the material.[39] In contrast, we find chemical reduction via hydrazine vapor more effectively removes fluorine while retaining carbon. The reduction via hydrazine likely proceeds as $4CF_n + nN_2H_4 \rightarrow 4C + 4nHF + 2nN_2$, which suggests low temperature chemical reduction schemes will result in "higher-quality" recovery.[5]

The measurement of field-effect transistors (FETs) during the fluorination process shows the film resistance increases over 6 orders of magnitude with fluorination up to C_4F. Figure 4C shows the typical changes in the gate characteristics of a graphene FET after exposure to XeF_2 gas. The ambipolar behavior is still observed after a 120 s XeF_2 exposure, though the Dirac point has shifted positive and the resistance increased 3 orders of magnitude. The exact origin of the positive Dirac point shift, from either intrinsic or extrinsic doping, is currently unknown since these samples were measured in air, where, for example, water and O_2 can unintentionally p-type dope graphene and decrease the electron mobility over the hole mobility.[13,40] After a 240 s exposure, the device resistance increased beyond the semiconductor parametric analyzer range of >1 GΩ. Importantly, regions protected from fluorination retain their original mobility and can be used for conductive pathways and devices. Exposing this same fluorinated device to hydrazine for 18 h restores much of the conductivity and the ambipolar behavior as shown in Figure 4D. After defluorination the FET mobilities typically ranged between 4 and 20 $cm^2/(V\ s)$, which is consistent with residual disorder seen from Raman spectroscopy (Figure 4A).

Fluorine modifies the electronic properties of graphene by reducing the charge in the conducting π orbitals, by introducing scattering centers, and by opening band gaps. These effects are consistent with the reduction of conductivity and reduction of the mobility seen in experiment in Figure 4C. Our density of states calculations for graphene with varying F coverages are shown in Figure 3C. For increasing F coverage the band gap widens and the Fermi level is lowered in the valence band. These effects are due to interaction of the p orbitals of F with the π orbitals of C producing sp^3 bonds that modify the charge densities and introduce scattering centers for conduction. In particular, in the case of C_4F (from Figure 3B) the band gap is 2.93 eV and has the π bands largely disrupted, giving rise to π resonances surrounded by sp^3 bonded C atoms. Optical transparency is expected for a material with a 2.93 eV band gap, which is consistent with our observations in Figure 1B. Together these results indicate that even a relatively low ordered coverage of fluorine can open an appreciable band gap in graphene. Therefore, single-side fluorination should be sufficient to considerably modify the transport properties of graphene-based devices.

In conclusion, we have demonstrated the synthesis and facile patterning of fluorinated graphene via XeF_2 gas exposure. Spectroscopic techniques and atomic force microscopy show XeF_2 treatment fluorinates graphene without etching. Fluorination of the graphene lattice significantly changes the optical, structural, and transport properties of the material. Fluorine adatom addition saturates at C_4F for one-sided fluorination, which is found to be the lowest energy configuration from DFT calculations. The calculated band gap for C_4F is 2.93 eV and experiment shows the material becomes optically transparent at this coverage. When graphene is deposited on a SOI substrate, XeF_2 etching of the Si underlayer allows XeF_2 access to both sides of the graphene film and formation of perfluorographane (CF). We expect the techniques described here to further broaden the graphene's utility in electronic, optical, and sensing technologies.

Acknowledgment. J.T.R. would like to thank R. S. Ruoff and X. Li for hosting a visit to The University of Texas at Austin and for fruitful discussions of graphene growth on copper and P. Campbell for assistance in fabricating devices and for a critical reading of this manuscript. This research was performed while J.S.B. and C.E.J. held a National Research Council Research Associateship Award at the Naval Research Laboratory. This work was supported in part by the Office of Naval Research and NRL's Nanoscience Institute.

Supporting Information Available. Details of defluorination of graphene. This material is available free of charge via the Internet at http://pubs.acs.org.

REFERENCES AND NOTES

(1) Ruff, O.; Bretschneider, O.; Ebert, F. *Z. Anorg. Allgm. Chem.* **1934**, *217* (1), .
(2) Palin, D. E.; Wadsworth, K. D. *Nature* **1948**, *162*, 925.
(3) Lagow, R. J.; Badachhape, R. B.; Wood, J. L.; Margrave, J. L. *J. Chem. Soc., Dalton Trans.* **1974**, 1268–1273.
(4) Taylor, R.; Holloway, J. H.; Hope, E. G.; Avent, A. G.; Langley, G. J.; Dennis, T. J.; Hare, J. P.; Kroto, H. W.; Walton, D. R. M. *J. Chem. Soc., Chem. Commun.* **1992**, *9*, 665.

DOI: 10.1021/nl101437p | *Nano Lett.* **2010,** *10,* 3001–3005

(5) Mickelson, E. T.; Huffman, C. B.; Rinzler, A. G.; Smalley, R. E.; Hauge, R. H.; Margrave, J. L. *Chem. Phys. Lett.* **1998**, *296*, 188–194.
(6) Pehrsson, P. E.; Zhao, W.; Baldwin, J. W.; Song, C.; Liu, J.; Kooi, S.; Zheng, B. *J. Phys. Chem. B* **2003**, *107* (24), 5690–5695.
(7) Bettinger, H. F. *ChemPhysChem* **2003**, *4* (12), 1283–1289.
(8) Fusaro, R. L.; Sliney, H. E. *ASLE Trans.* **1970**, *13* (1), 56–65.
(9) Kamarchik, P.; Margrave, J. L. *J. Therm. Anal. Calorim.* **1977**, *11* (2), 259–270.
(10) Kita, Y.; Watanabe, N.; Fujii, Y. *J. Am. Chem. Soc.* **1979**, *101* (14), 3832–3841.
(11) Charlier, J. C.; Gonze, X.; Michenaud, J. P. *Phys. Rev. B* **1993**, *47* (24), 16162.
(12) Zajac, A.; Pelikán, P.; Minár, J.; Noga, J.; Straka, M.; Banacký, P.; Biskupic, S. *J. Solid State Chem.* **2000**, *150* (2), 286–293.
(13) Novoselov, K. S.; Geim, A. K.; Morozov, S. V.; Jiang, D.; Zhang, Y.; Dubonos, S. V.; Grigorieva, I. V.; Firsov, A. A. *Science* **2004**, *306* (5696), 666–669.
(14) Geim, A. K.; Novoselov, K. S. *Nat. Mater.* **2007**, *6* (3), 183–191.
(15) Fuhrer, M. S.; Lau, C. N.; MacDonald, A. H. *MRS Bull.* **2010**, *35*, 289–294.
(16) Khare, B. N.; Wilhite, P.; Meyyappan, M. *Nanotechnology* **2004**, *15* (11), 1650–1654.
(17) Felten, A.; Bittencourt, C.; Pireaux, J. J.; Van Lier, G.; Charlier, J. C. *J. Appl. Phys.* **2005**, *98* (7), No. 074308−9.
(18) Unger, E.; Liebau, M.; Duesberg, G. S.; Graham, A. P.; Kreupl, F.; Seidel, R.; Hoenlein, W. *Chem. Phys. Lett.* **2004**, *399* (1−3), 280–283.
(19) Li, X.; Cai, W.; An, J.; Kim, S.; Nah, J.; Yang, D.; Piner, R.; Velamakanni, A.; Jung, I.; Tutuc, E.; Banerjee, S. K.; Colombo, L.; Ruoff, R. S. *Science* **2009**, 1171245.
(20) Ishigami, M.; Chen, J. H.; Cullen, W. G.; Fuhrer, M. S.; Williams, E. D. *Nano Lett.* **2007**, *7* (6), 1643–1648.
(21) Robinson, J. T.; Perkins, F. K.; Snow, E. S.; Wei, Z.; Sheehan, P. E. *Nano Lett.* **2008**, *8* (10), 3137–3140.
(22) Giannozzi, P.; Bonini, S. B., N.; Calandra, M.; Car, R.; Cavazzoni, C.; Ceresoli, D.; Chiarotti, G. L.; Cococcioni, M.; Dabo, I.; Dal Corso, A.; Fabris, S.; Fratesi, G.; de Gironcoli, S.; Gebauer, R.; Gerstmann, U.; Gougoussis, C.; Kokalj, A.; Lazzeri, M.; Martin-Samos, L.; Marzari, N.; Mauri, F.; Mazzarello, R.; Paolini, S.; Pasquarello, A.; Paulatto, L.; Sbraccia, C.; Scandolo, S.; Sclauzero, G.; Seitsonen, A. P.; Smogunov, A.; Umari, P.; Wentzcovitch, R. M. *J. Phys.: Condens. Matter* **2009**, *21*, 395502.
(23) We used the pseudopotentials C.pbe-van_ak.UPF and F.pbe-n-van.UPF from http://www.quantum-espresso.org.
(24) Castro Neto, A. H.; Guinea, F.; N. M. R.; Peres; Novoselov, K. S.; Geim, A. K. *Rev. Mod. Phys.* **2009**, *81*, 109–162.
(25) Peres, N. M. R.; Tsai, S.-W.; Santos, J. E.; Ribeiro, R. M. *Phys. Rev. B* **2009**, *79*, 155442.
(26) Kamarchik, P.; Margrave, J. L. *Acc. Chem. Res.* **1978**, *11* (8), 296–300.
(27) Gaskell, P. E.; Skulason, H. S.; Rodenchuk, C.; Szkopek, T. *Appl. Phys. Lett.* **2009**, *94* (14), 143101–3.
(28) Nair, R. R.; Blake, P.; Grigorenko, A. N.; Novoselov, K. S.; Booth, T. J.; Stauber, T.; Peres, N. M. R.; Geim, A. K. *Science* **2008**, 1156965.
(29) Winters, H. F.; Coburn, J. W. *Appl. Phys. Lett.* **1979**, *34* (1), 70–73.
(30) Dale, E. I.; Daniel, L. F.; John, A. M.; Vincent, M. D. *Appl. Phys. Lett.* **1984**, *44* (12), 1129–1131.
(31) Lee, J.-M.; Kim, S. J.; Kim, J. W.; Kang, P. H.; Nho, Y. C.; Lee, Y.-S. *J. Ind. Eng. Chem.* **2009**, *15* (1), 66–71.
(32) For C_4F with 25% coverage, two arrangements of 2 F atoms per 4 graphene unit cells were considered; for C_2F with 50% coverage, two arrangements of a F atom in 4 unit cells were considered; $C_{32}F$ for 3.13% coverage has 1 F atom in 16 unit cells; $C_{128}F$ for 0.78% coverage has 1 F atom in 64 unit cells. There is evidence that the electronics properties of the graphene systems are largely unaffected by the Cu substrate.[41]
(33) Ewels, C. P.; Van Lier, G.; Charlier, J.-C.; Heggie, M. I.; Briddon, P. R. *Phys. Rev. Lett.* **2006**, *96* (21), 216103.
(34) Kelly, K. F.; Chiang, I. W.; Mickelson, E. T.; Hauge, R. H.; Margrave, J. L.; Wang, X.; Scuseria, G. E.; Radloff, C.; Halas, N. J. *Chem. Phys. Lett.* **1999**, *313* (3−4), 445–450.
(35) Ferrari, A. C.; Robertson, J. *Philos. Trans. R. Soc. London, Ser. A* **2004**, *362* (1824), 2477–2512.
(36) Dresselhaus, M. S.; Jorio, A.; Hofmann, M.; Dresselhaus, G.; Saito, R. *Nano Lett.* **2010**, *10* (3), 751–758.
(37) Zhou, J.; Wu, M. M.; Zhou, X.; Sun, Q. *Appl. Phys. Lett.* **2009**, *95* (10), 103108–3.
(38) For the devices measured here the typical FET mobilities were ~1000 cm^2/V s, which is less than that originally reported for chemical vapor deposition graphene growth on Cu.[19] This discrepancy is likely due to the larger channel length here (15 μm compared to ~2 μm), where more defects such as domain boundaries and wrinkles are likely present.
(39) Kuriakose, A. K.; Margrave, J. L. *Inorg. Chem.* **1965**, *4* (11), 1639–1641.
(40) Lohmann, T.; von Klitzing, K.; Smet, J. H. *Nano Lett.* **2009**, *9* (5), 1973–1979.
(41) Giovannetti, G.; Khomyakov, P. A.; Brocks, G.; Karpan, V. M.; van den Brink, J.; Kelly, P. J. *Phys. Rev. Lett.* **2008**, *101*, No. 026803.

DOI: 10.1021/nl101437p | *Nano Lett.* **2010,** *10,* 3001–-3005